Fuel 404 (2026) 136200

Contents lists available at ScienceDirect

Fuel

journal homepage: www.elsevier.com/locate/jfue

Full length article

Hydrogen storage in modified iron oxides: The effect of additives on the cyclic stability

A. Knapp[1], C. Kuhn[1], O. Deutschmann*

Institute for Chemical Technology and Polymer Chemistry, Karlsruhe Institute of Technology (KIT), Engesserstr. 20, Karlsruhe, 76131, Germany

HIGHLIGHTS

- Iron oxide modification with Ce, Mo, and Al improves the cyclic stability of hydrogen production in the steam-iron process.
- The synthesis method is decisive; impregnation increases the additive concentration on the particle surface and reduces agglomeration.
- Mo enhances the hydrogen storage capacity due to its redox behavior.
- Iron oxide impregnated with Mo maintains 72 % of its initial hydrogen storage capacity after 50 cycles of hydrogen storage and release, demonstrating superior cyclability compared to non-modified iron oxide.

GRAPHICAL ABSTRACT

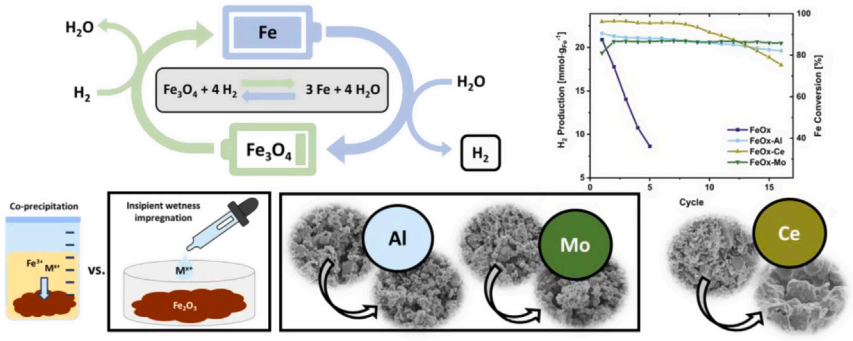

ARTICLE INFO

Keywords:
Hydrogen storage
Iron
Oxidation
Additives
Cyclability

ABSTRACT

In the steam-iron process the indirect storage and release of hydrogen are achieved through the cyclic reduction of Fe_3O_4 with hydrogen to iron and the oxidation of iron with water vapor to produce hydrogen. Its primary challenge is the decreasing activity with an increasing number of cycles due to sintering. In this work, the effect of adding Ce, Mo, and Al on the cyclic stability was investigated in a fixed bed reactor using metal oxide powder with a particle size of 100–200 μm. Mo exhibits the most stable performance across multiple cycles. This can be attributed to the mitigation of sintering and the ability of molybdenum to store and release hydrogen. In addition to the additive, the synthesis method also plays a decisive role. The synthesis of the modified iron oxide particles via impregnation leads to a higher additive concentration on the particle surface, thereby reducing sintering compared to iron oxide produced by co-precipitation. Iron oxide impregnated with Mo maintains 72 % of its initial hydrogen storage capacity after 50 cycles of hydrogen storage and release, demonstrating superior cyclability compared to unmodified iron oxide.

1. Introduction

The transition to renewable energy sources represents a significant step in reducing dependence on fossil fuels. The generation of renewable energy, such as solar and wind power, is subject to significant temporal and seasonal fluctuations, thereby raising the need for efficient energy storage solutions. In this context, green hydrogen produced by water electrolysis has emerged as a promising energy carrier due to its high

* Corresponding author.
Email address: deutschmann@kit.edu (O. Deutschmann).
[1] A.K. and C.K. contributed equally.

https://doi.org/10.1016/j.fuel.2025.136200
Received 27 February 2025; Received in revised form 19 May 2025; Accepted 3 July 2025
Available online 21 July 2025

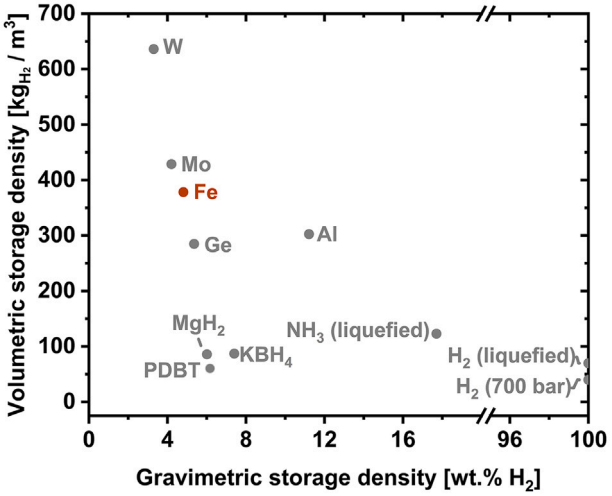

Fig. 1. Gravimetric and volumetric hydrogen storage density of different hydrogen storage technologies. Data was taken from [3,5,6]. Volumetric hydrogen storage densities of the metals were calculated based on their density and their stoichiometric hydrogen production.

gravimetric energy density (33 kWhkg^{-1}) [1,2]. Due to hydrogen's low volumetric energy density, it must be compressed to high pressures (up to 700 bar) or liquefied for storage, both of which increase costs and reduce storage efficiency. Additionally, its high reactivity poses significant challenges and risks in handling [3,4].

Several hydrogen storage options are currently under discussion (Fig. 1) [7]. Ammonia is considered a promising hydrogen carrier due to its high hydrogen storage density of 17.8 wt.–% [8], which means that 1 kg of ammonia can store 178 g of hydrogen. However, ammonia comes with disadvantages such as toxicity, corrosiveness, and the presence of trace amounts of NH_3 in the hydrogen after decomposition [9]. Another option under consideration is the utilization of Liquid Organic Hydrogen Carriers (LOHCs). These organic liquids can undergo a fully reversible catalytic hydrogenation/dehydrogenation cycle without emitting CO_2, such as benzene or toluene derivatives [10]. They can be handled similarly to gasoline or diesel, using existing fossil fuel infrastructure for storage and transport. LOHCs exhibit high hydrogen storage densities; for instance, the dibenzyltoluene-perhydro-dibenzyltoluene (DBT-PDBT) system has a hydrogen storage density of 6.2 wt.–% [3]. However, they require high hydrogen pressures for storage and elevated temperatures for hydrogen release (10–50 bar, > 250 °C for DBT-PDBT) [10]. Additionally, several LOHC compounds are volatile, flammable, and may pose toxicity concerns, especially those based on benzene or toluene derivatives [11,12]. Promising solid-state alternatives for hydrogen storage are metal hydrides and complex hydrides such as KBH_4 [13]. Many metals react with hydrogen to form metal hydrides, which can release hydrogen when they are heated or when the external pressure is reduced [14]. Among the metal hydrides MgH_2 is most suitable for large-scale hydrogen storage, as it possesses a hydrogen storage density of 7.6 wt.–% [15] and magnesium is abundant. However, high hydrogen pressures are required (above 30 bar for MgH_2) to form the metal hydrides and they suffer from slow hydrogen absorption and release kinetics [15]. Several metal hydrides are sensitive to oxygen and may burn in case of exposure to air, which raises safety concerns [16].

An alternative to the direct hydrogen storage methods mentioned above is the indirect storage of hydrogen. In contrast to direct hydrogen storage, this method is characterized by its independence from pressure [17]. In this context, metals have recently gained attention as carbon-free chemical energy carriers due to their high gravimetric energy density, making them suitable for large-scale energy storage [18–26]. Certain metals can react with steam to generate hydrogen and the corresponding metal oxide through the metal-steam process. This process can serve as a closed hydrogen storage cycle if the metal oxide can be reduced with hydrogen.

Aluminum (Al) is considered a promising hydrogen storage medium due to its high gravimetric energy density and its ability to react with water to release hydrogen and heat [27–30]. However, to produce hydrogen, aluminum may require processing into alloys or nanostructures to enhance activation, as its surface oxide layer can impede the process [31]. Additionally, the alumina formed during oxidation cannot be reduced by hydrogen [6], which limits its application in a circular hydrogen storage system. As an alternative reduction method, electrolysis can be used to reduce aluminum oxide to aluminum. However, this process requires melting the aluminum oxide, necessitating additional steps after reduction. As a result, these additional processing steps increase both the cost and energy demand for hydrogen storage in aluminum.

Other metal/metal oxide systems can be considered for the metal-steam process, provided the possibility of reduction with hydrogen and oxidation with steam. [6] proposed molybdenum (Mo), germanium (Ge), tungsten (W) and iron (Fe), as potential candidates for use in the metal-steam process. These metals are capable of releasing hydrogen when oxidized with water, and their oxides can be reduced with hydrogen below 1300 °C. Out of these metals germanium has the highest hydrogen storage density (5.5 wt.–%) followed by iron (4.8 wt.–%) (Fig. 1) Thaler and Hacker [6]. For the process to be economical, the material for hydrogen storage must be inexpensive and available in large quantities. The raw material costs of tungsten, molybdenum and germanium (358–36,037 \$/kg$_{H_2}$) are significantly higher than the cost of iron ((4 \$/kg$_{H_2}$) and even exceed the estimated cost of a hydrogen storage vessel (200–333 \$/kg$_{H_2}$) [17]. Furthermore, iron and its oxides are not hazardous to health or the environment and iron is the fourth most common element in the Earth's crust [32]. Thus, among these metals, the iron/iron oxide system stands out as the most suitable candidate for large-scale hydrogen storage owing to its high availability, affordability, ease of use, and non-toxic nature [17].

One of the earliest methods of producing hydrogen relied on the reaction of iron with steam. The steam-iron process was first employed on a commercial scale at the beginning of the 19th century [33,34]. In this process, synthesis gas obtained by coal gasification was used to reduce the iron oxide. The periodic steam-iron process was operated for hydrogen production, however the more cost-effective production of hydrogen from gaseous and liquid hydrocarbons replaced the steam-iron process [35]. The need for seasonal hydrogen storage has renewed interest in the steam-iron process, using hydrogen instead of fossil fuel for iron oxide reduction [36–38].

A schematic representation of the steam-iron process is shown in Fig. 2. Hydrogen storage occurs through the reduction of iron oxide (Fe_3O_4) with hydrogen. The resulting iron can be oxidized with water vapor, generating high-purity hydrogen (Eq. 1). In the presence of water, the most thermodynamically stable iron oxide product is magnetite (Fe_3O_4) [39]. Fig. 3 illustrates the phase equilibrium between iron and the iron oxides as a function of temperature and the hydrogen/water gas mixture.

$$3Fe + 4H_2O(g) \rightleftharpoons Fe_3O_4 + 4H_2 \quad (1)$$

The steam-iron process is a cyclic system that could potentially be decoupled not only temporally but also spatially. Reduction with green hydrogen can take place in locations with abundant renewable energy and the resulting iron can be transported to populated or industrial areas, where hydrogen can be released and iron oxide collected for transport back to the reduction site [40].

The hydrogen storage density of the iron/iron oxide system is comparable to that of liquid organic hydrogen carriers (LOHCs) and metal hydrides (Fig. 1). However, in terms of energy requirements for hydrogen storage and release, iron is favorable compared to metal hydrides

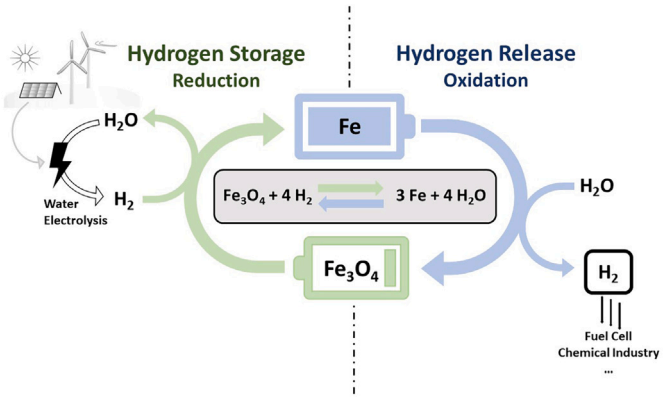

Fig. 2. Schematic representation of the steam-iron process. The process works as follows: to release hydrogen, iron is oxidized with steam, producing high-purity hydrogen. During hydrogen storage, the iron oxide formed is reduced with green hydrogen, resulting in a hydrogen storage cycle. (For interpretation of the references to colour in this figure legend, the reader is referred to the web version of this article.)

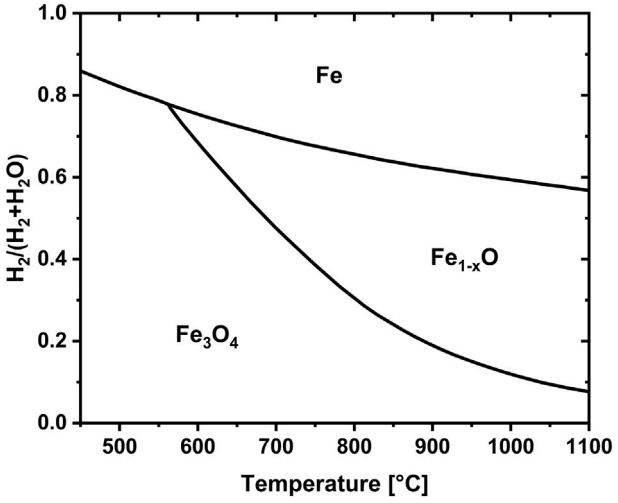

Fig. 3. Solid-phase equilibrium between iron and its oxides in the Fe–H–O system as a function of the composition of the gas atmosphere at atmospheric pressure. Adapted from [39].

and LOHCs, with an energy requirement of 9.0 $kWhkg_{Fe}^{-1}$, in comparison to 9.7 $kWhkg_{Fe}^{-1}$ for DBT-PDBT and 11 $kWhkg_{Fe}^{-1}$ for MgH_2 [17]. Furthermore, the steam-iron process enables the production of pure hydrogen that is suitable for use in fuel cells [41,42]. Due to the higher process temperature (350 °C–800 °C), it can be used in combination with solid oxide fuel cells [37]. This makes iron a promising candidate as a safe and cost-effective hydrogen vector. First large-scale applications of the steam-iron process have been demonstrated by Heiniger et al. [43], who successfully conducted a single storage cycle with a fixed-bed reactor filled with 250 kg of iron oxide, showcasing its feasibility for seasonal energy storage.

The challenge in the cyclic utilization of the iron/iron oxide system for hydrogen production lies in the diminishing reactivity with an increasing number of cycles, primarily attributable to sintering effects [44–46]. Recent studies concentrate on mitigating the decrease in activity by incorporating structural promoters [42,47–49].

Otsuka et al. [47] conducted the most extensive analysis of potential additives, examining 26 elements for their impact on both oxidation with water vapor and reduction with hydrogen. The experiments were performed in a fixed-bed with a linear heating rate of 7.5 K min^{-1} up to temperatures of 823 K and 873 K for reduction and oxidation, respectively. The cyclic stability of the system was analyzed based on experiments with up to five cycles. Among the elements studied, aluminum (Al), molybdenum (Mo), and cerium (Ce) were identified as promising additives to mitigate the decreasing activity caused by sintering. Wang et al. [50] and Takenaka et al. [51] confirmed the beneficial effect of Mo. However, the available literature varies significantly regarding the investigated process parameters and the synthesis methods used for the modified iron oxides [52–55]. Additionally, many studies consider only a limited number of cycles and do not adjust the cycle time to ensure the completion of the oxidation or reduction processes.

For a better understanding of the influencing parameters and to facilitate a detailed comparison of the additives, this study focuses on low additive loadings on iron oxide and moderate temperature operation, which is most suitable for application of the steam-iron process for hydrogen storage. A comprehensive investigation into the redox behavior of additives provides insights into their effects on performance, while the influence of synthesis methods on material properties is analyzed. Moreover, the study's long-term durability assessment, extending up to 50 cycles offers a robust and realistic perspective on the material's cyclic stability.

2. Materials and methods

2.1. Synthesis of the modified iron oxides

A series of iron oxides modified with Al, Ce or Mo were synthesized by co-precipitation (Al, Ce) and impregnation (Al, Ce, Mo). A concentration of 5 mol% of the total amount of metal cations was chosen as recent studies showed that it provides a balance between stability and hydrogen storage density, resulting in optimal performance for hydrogen storage [56].

Although this work primarily focused on investigating the fundamental effects of synthesis methods and additives on redox stability, the significance of practical considerations was acknowledged. Among the stabilizing additives highlighted in the literature, aluminum was specifically chosen with scalability in mind because of its abundance and low cost. Moreover, since the additives are used in low concentrations, their cost is generally secondary to that of the bulk iron oxide, making the approach potentially viable for large-scale implementation.

For the samples synthesized by co-precipitation an aqueous solution of $Fe(NO_3)_3$ (99.0 %–101.0 %, VWR Chemicals) and NH_4NO_3 (min. 97.9 %, Bernd Kraft) was prepared. The solution was mixed with an aqueous solution of either $Al(NO_3)_3{\cdot}9H_2O$ (min. 98.5 %, Merck) or $Ce(NO_3)_3{\cdot}6H_2O$ (99.9 %, ThermoFisher) with the desired additive concentration. The pH was adjusted to 7 by adding $NH_{3(aq)}$ while stirring vigorously. A voluminous, red-brown precipitate formed. The precipitate was heated to the boiling point, then cooled and aged for 48 h at room temperature. The precipitate was filtered and dried for 72 h at 75 °C. Subsequently, the samples were calcined at 700 °C for 5 h.

An aqueous solution of $Al(NO_3)_3{\cdot}9H_2O$ (min. 98.5 %, Merck), $Ce(NO_3)_3{\cdot}6H_2O$ (99.9 %, ThermoFisher), or $(NH_4)_6Mo_7O_{24}$ (min. 99.0 %, Merck) was used to impregnate commercial Fe_2O_3 (99.9 % metals basis, ThermoFisher). The samples were dried for 24 h at 75 °C and calcined for 5 h at 700 °C. The samples are referred to as FeOx-Al, FeOx-Ce, and FeOx-Mo. It should be noted that these names do not correspond to their actual composition. It is assumed that after synthesis, all metals are present as oxides in their highest oxidation state, namely Fe_2O_3, CeO_2, MoO_3, and Al_2O_3.

The redox activity of the additives Ce and Mo was tested by impregnating Al_2O_3 (Sasol) using the same procedure as described above. Al_2O_3 was calcined for 5 h at 500 °C prior to impregnation.

All samples were pressed into pellets and crushed. The sieve fraction of 100–200 µm was collected and used for all thermogravimetric analyses and investigations of the cyclic redox performance.

Table 1
Additive concentration of Al-, Ce- and Mo-doped iron oxides synthesized by impregnation determined with ICP-OES.

	ICP-OES [mol%]
FeOx-Al	5.14 ± 0.12
FeOx-Ce	4.76 ± 0.05
FeOx-Mo	5.07 ± 0.08

Elemental analysis through ICP-OES (Table 1) showed that the iron oxides contained the additives close to the target concentration, with the greatest deviation in samples containing cerium. The relative deviation of the actual concentration from the target concentration was less than 2.7 % for all additives analyzed.

2.2. Evaluation of the hydrogen storage performance

The cyclic reduction and oxidation of the modified iron oxides were investigated in a fixed-bed tubular reactor (Fig. 4a). 500 ± 3 mg of the modified Fe_2O_3 powder was filled into a quartz glass reactor (8 mm i.d.) and fixed with glass wool, creating a fixed-bed with a length of 5–8 mm. The reactor was placed in a furnace (HTM Reetz) for uniform heating. The temperature was monitored by two N-type thermocouples positioned 1 mm downstream and upstream of the fixed-bed. The gases H_2 and N_2 were dosed by mass flow controllers (MFC, Bronkhorst), while water was dosed by a Liquiflow (LFC, Bronkhorst) and vaporized using a Controlled Evaporation Mixer (CEM, Bronkhorst). All experiments were conducted with a constant total volume flow of 300 mlmin^{-1} under standard conditions. The reduction step in the cycling experiments was carried out with 5 vol. − % H_2, and the oxidation with 20 vol. − % H_2O balanced with N_2. Before each experiment and between each cycle, the reactor was flushed with N_2 for 10 min to ensure complete removal of the reactive gases (Fig. 4b). The hydrogen concentration of the exhaust gas was analyzed with a mass spectrometer (HSense, V&F) to monitor the progress of the reaction. The acquired experimental data were managed using Adacta [57].

In addition to the experiments in the fixed-bed reactor the reduction was analyzed based on thermogravimetric experiments (Netzsch STA409). The non-isothermal experiments were performed with a heating rate of 10 K min^{-1} up to 800 °C with 5 vol. − % H_2 in N_2. The volume flux was set to 100 mlmin^{-1}. For each experiment 20 ± 2 mg of iron oxide powder was utilized. To enable comparison of the reduction results for iron oxide with different additives, the mass loss was normalized to the mass of Fe_2O_3 in the sample.

Table 2
Overview of the performed experiments for each sample.

Sample	Steam-iron experiments			TGA
	5 cycles	16 cycles	50 cycles	1st reduction
FeOx	x			
FeOx-Al pre.	x			
FeOx-Ce pre.	x			
FeOx-Al	x	x		
FeOx-Ce	x	x		x
FeOx-Mo	x	x	x	x
Al_2O_3–Ce	x			
Al_2O_3–Mo	x			

An overview of the experiments conducted is provided in Table 2. All steam-iron process experiments were carried out at 600 °C to achieve an effective compromise between material stability and reaction kinetics. This temperature was selected based on the findings of Brinkman et al. [17], who emphasized the benefits of lower operating temperatures for steam-iron processes in the context of hydrogen and energy storage applications. Although higher temperatures can enhance conversion rates, they also promote sintering and accelerate the degradation of oxygen carrier materials. Given that the primary objective of this study was to evaluate the long-term redox stability of the materials, 600 °C was considered the most suitable operating temperature. This study focused on the oxidation step, as the reduction behavior of iron-based carriers has already been extensively investigated in the literature [58–61]. Assessing the hydrogen release during oxidation provides a clear measure of redox performance and material degradation. Since deactivation affects both reduction and oxidation, monitoring the oxidation step alone offers a reliable indication of overall stability. The reduction step will be the subject of future investigations.

2.3. Characterization

For a more comprehensive understanding, the samples were characterized using additional techniques.

2.3.1. XRD analysis

XRD analysis was performed to determine the phase composition using a Bruker D8 Advance with Cu-K_α (λ = 1.540562 Å) (KIT, ITCP and IMB) or Co-K_α (λ = 1.7889 Å) (TU Freiberg) sources. To ensure comparability, the XRD spectra obtained with the Co-K_α source were converted to the corresponding Cu-K_α scattering patterns using PowDLL [62]. The reference spectra used to analyze the XRD spectra were taken from the ICSD database for inorganic crystal structures [63].

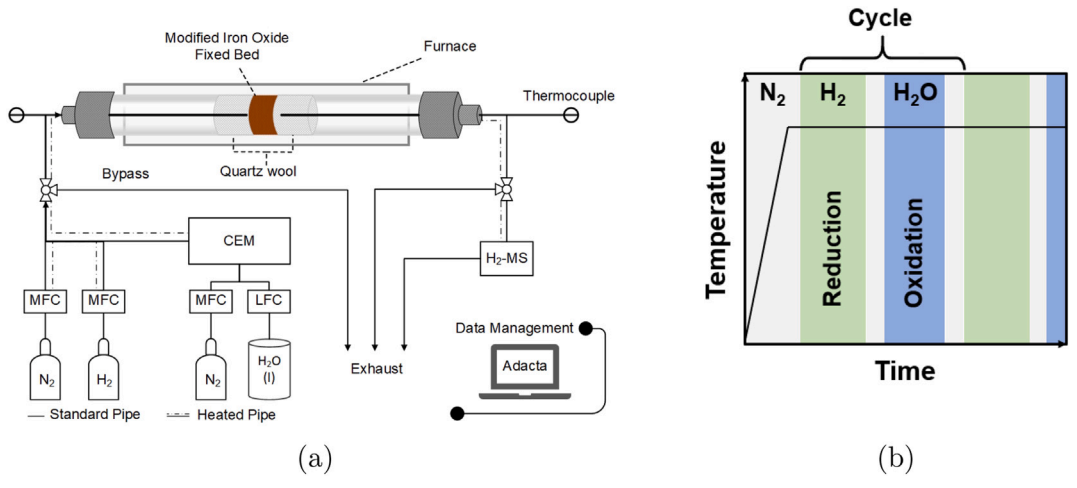

Fig. 4. Schematic representation of the experimental setup (a) and method (b) for the evaluation of the hydrogen storage performance.

2.3.2. ICP-OES elemental analysis

The elemental composition of the samples was determined using inductively coupled plasma optical emission spectrometry (ICP-OES) to precisely quantify the amount of additive.

2.3.3. Specific surface area

The specific surface area was measured using a Belsorp Mini II device from Bel Japan Inc. The analysis was performed using 300–500 mg of each sample. Pretreatment of the samples was performed at 300 °C in vacuum for three hours to remove adsorbed substances.

2.3.4. SEM characterization

Scanning electron microscopy images of selected samples were taken using a Zeiss LEO 1530 Gemini with an acceleration voltage of 5 keV. The powders were fixed on a carbon tape and coated with carbon.

3. Results and discussion

The results of the influence of the synthesis method, the additive, and the cyclization are presented in the following section. The present study focuses on the oxidation process. For enhanced comparability, the amount of H_2 produced, n_{H_2}, is normalized to the mass of iron. The theoretical maximum amount of hydrogen that can be produced $n_{H_2,max}$ through the complete oxidation of Fe to Fe_3O_4 is 23.9 mmol g_{Fe}^{-1}. Additionally, the Fe conversion X_{Fe} during oxidation is given (Eq. 2). An Fe conversion of 0 % corresponds to Fe and 100 % conversion corresponds to Fe_3O_4.

$$X_{Fe} = \frac{n_{H_2}}{n_{H_2,max}} \cdot 100 \quad (2)$$

3.1. Influence of the synthesis method

In order to gain a deeper understanding of the influence of the synthesis method, FeOx-Al and FeOx-Ce samples were synthesized using both precipitation and impregnation techniques. Both synthesis methods applied in this work are well-established practices and are commonly used in industrial-scale catalyst production [64].

Cyclic experiments with up to five cycles were performed with a reduction time of 140 min and an oxidation time of 30 min. The amount of hydrogen produced during oxidation of FeOx-Al and FeOx-Ce synthesized by impregnation and co-precipitation is depicted in Fig. 5.

In the first cycle, the hydrogen production of the FeOx-Al sample synthesized by precipitation is higher than that of the sample synthesized by impregnation. However, with values of 20 mmol g_{Fe}^{-1} and 22 mmol g_{Fe}^{-1} respectively, both these values are below the theoretical value of 23.9 mmol g_{Fe}^{-1}.

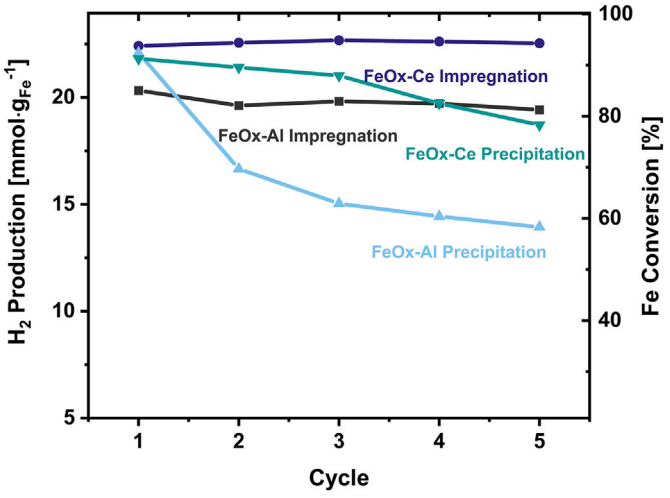

Fig. 5. Effect of the synthesis method on the oxidation of FeOx-Al and FeOx-Ce over five cycles. The theoretical amount of H_2 produced by complete oxidation of Fe to Fe_3O_4 equals 23.9 mmol g_{Fe}^{-1}.

With increasing cycle number the hydrogen production of the precipitation-synthesized sample decreases strongly by around 37 % to 14 mmol g_{Fe}^{-1}, while the activity of the sample synthesized by impregnation remains nearly constant. A similar trend was observed for iron oxide modified with Ce, although it was less pronounced. The impregnated sample maintained a constant H_2 production, whereas the precipitation-synthesized sample exhibited a 14 % decrease in hydrogen production over five cycles.

This comparison indicates that the synthesis method significantly influences the performance of the sample, irrespective of the additive used. Sintering is presumed to be the primary cause of the observed decrease in reactivity with an increasing number of cycles. The incorporation of a suitable additive can mitigate sintering by reducing contact between individual particles, as structural promoters inhibit surface migration and the interaction of atoms within the active phase [65]. A possible explanation for the consistent reactivity of the sample produced by impregnation over several cycles is the distribution of the additive within the particles. The enhanced stability of impregnated samples likely arises from the localization of the additive on the particle surface, resulting in a higher surface concentration compared to precipitated samples, where the additive is dispersed throughout the bulk and surface [66–68]. The higher surface concentration of impregnated samples more effectively inhibits particle sintering. This enhances structural stability under operating conditions. Although additives are incorporated in small quantities and the overall cost is predominantly governed by the bulk iron content, the impregnation method provides an additional benefit for potential large-scale applications: it enables targeted deposition of the additives at the particle surface, where they prevent sintering most effectively, thereby minimizing unnecessary incorporation into the bulk.

The findings highlight the significance of the synthesis method in enhancing the performance and long-term stability of doped iron oxides in hydrogen production applications. Further experiments were conducted solely with the impregnated samples due to their high stability in the short-term cycling experiments.

3.2. Effect of the additive on the cyclability

The influence of the additives Mo, Ce, and Al on the oxidation reactivity was evaluated over 16 cycles at a temperature of 600 °C. For comparison, a reference experiment using unmodified iron oxide (FeOx) was conducted, consisting of 5 cycles under identical conditions. Fig. 6 presents a comparison of the hydrogen formation during oxidation at one, five, and sixteen cycles for the different iron oxide samples. The corresponding $H_2 \setminus (H_2 + H_2O)$ ratio during the oxidation is shown in Fig. A.18.

The data indicate that all samples exhibit a rapid initial oxidation phase, followed by a gradual decline over time. In the first cycle, the peak hydrogen production rate during the initial oxidation is 4.5 mmol $min^{-1} g_{Fe}^{-1}$ for the FeOx, FeOx-Al, and FeOx-Ce samples. In contrast, the Mo-modified sample exhibits a slightly lower peak rate of 3.8 mmol $min^{-1} g_{Fe}^{-1}$. The hydrogen production rate of the unmodified iron oxide exhibits a rapid decline following the initial oxidation, stabilizing at approximately 1 mmol $min^{-1} g_{Fe}^{-1}$ and ceasing entirely after 20 min. The hydrogen production rate shows a secondary peak after 15 min, which is attributed to a fluctuation in the water evaporation system and does not reflect the redox behavior of the material.

In contrast, the modified iron oxides exhibit a significantly slower decline in hydrogen production rate following the initial oxidation, with a decrease that is almost linear. Furthermore, the incorporation of aluminum and molybdenum reduces the oxidation duration to 15 min. As the number of cycles increases, the hydrogen production rate of the unmodified iron oxide (FeOx) decreases significantly.

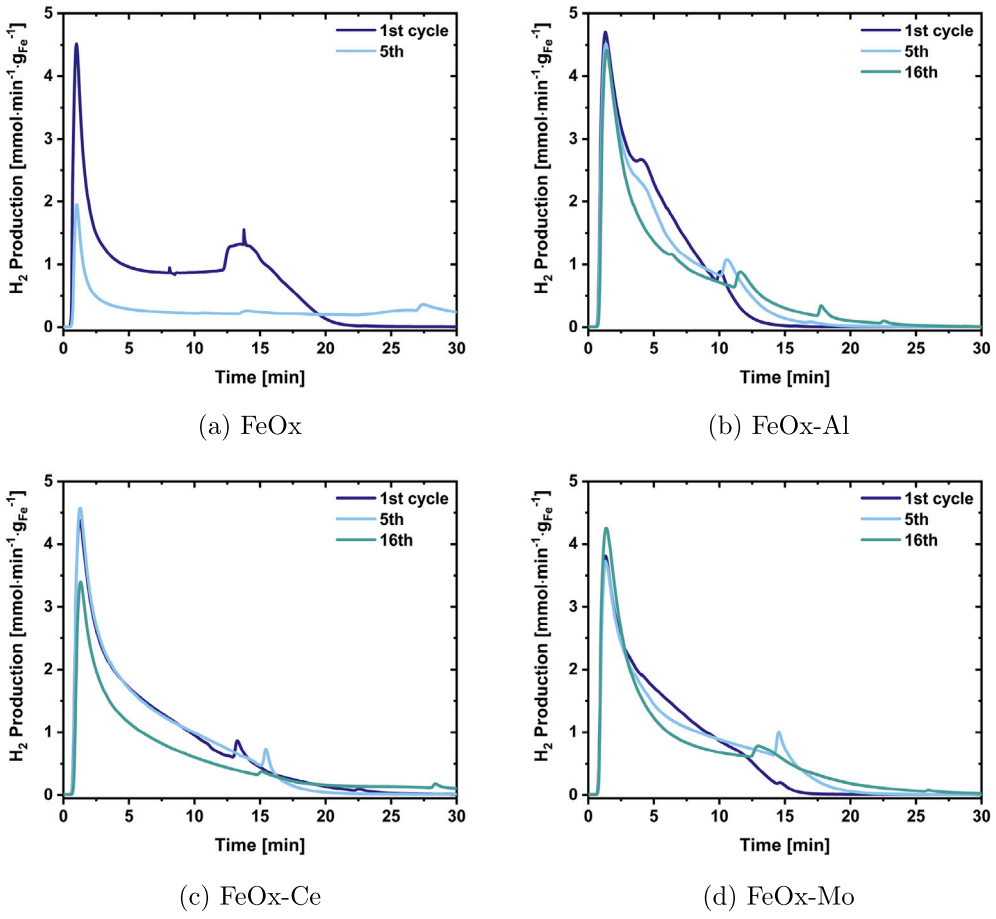

Fig. 6. Hydrogen production of the none-modified iron oxide and the modified iron oxides by oxidation with 20 vol. − % H_2O at 600 °C over time.

Due to rapid degradation, the unmodified iron oxide was tested for only five cycles.

By the fifth cycle, the initial oxidation produces only 2 mmol $min^{-1}g_{Fe}{}^{-1}$, stabilizing at 0.5 mmol $min^{-1}g_{Fe}{}^{-1}$ thereafter. In contrast, the oxidation behavior of the modified iron oxides changes only slightly with an increasing number of cycles. For FeOx-Al and FeOx-Mo, a stable initial hydrogen production rate and a slight increase in oxidation duration are observed, whereas for FeOx-Ce, the peak hydrogen production rate during the initial oxidation phase decreases with an increasing number of cycles.

To facilitate a better comparison of the hydrogen storage performance of the modified oxides, the amount of hydrogen released per cycle was calculated for each sample (Fig. 7). For the unmodified iron oxide (FeOx), a significant decrease in hydrogen production is observed with an increasing number of cycles. In the first cycle, approximately 21 mmol $g_{Fe}{}^{-1}$ is produced, but by the fifth cycle, this value drops to only 9 mmol $g_{Fe}{}^{-1}$, representing a decrease of around 60 %. In contrast, the addition of all three additives stabilizes hydrogen production over multiple cycles. FeOx-Mo and FeOx-Al produce about 20 mmol $g_{Fe}{}^{-1}$ per cycle. The hydrogen production of FeOx-Al decreases slightly with an increasing number of cycles, while it remains approximately constant for FeOx-Mo. The cerium-modified iron oxide (FeOx-Ce) initially produces a larger amount of hydrogen, approximately 23 mmol $g_{Fe}{}^{-1}$, which is close to the maximum theoretical amount of 23.9 mmol $g_{Fe}{}^{-1}$. The hydrogen formation remains relatively constant until the eighth cycle, after which it decreases linearly, falling below the production levels of FeOx-Mo and FeOx-Al by the sixteenth cycle. Although the 16-cycle FeOx-Ce test was conducted once, repeated five-cycle experiments demonstrated excellent reproducibility (Fig. A.17). Moreover, a pronounced densification of FeOx-Ce was also visually observed. Given the consistent preparation and testing protocols applied to all samples, this behavior was attributed to the specific influence of cerium as an additive.

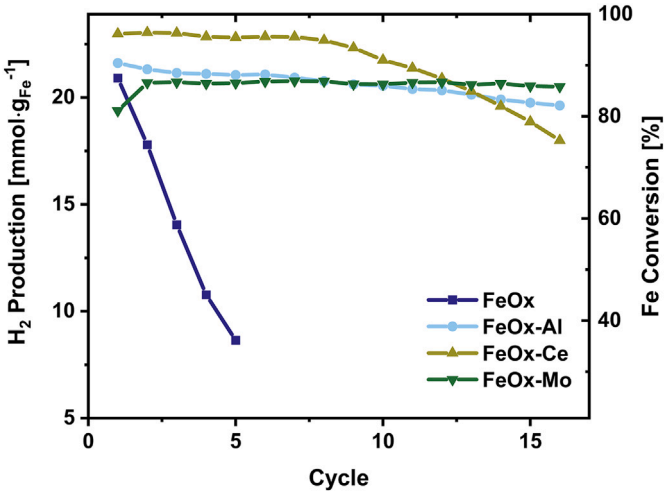

Fig. 7. Accumulated hydrogen production of the unmodified (FeOx) and the modified iron oxides per cycle in the oxidation step. The theoretical amount of H_2 produced by complete oxidation of Fe to Fe_3O_4 equals 23.9 mmol $g_{Fe}{}^{-1}$.

The samples were analyzed by X-ray diffraction (XRD) after 5 and 16 cycles (Figs. 8 and 9). The XRD results indicate that the unmodified

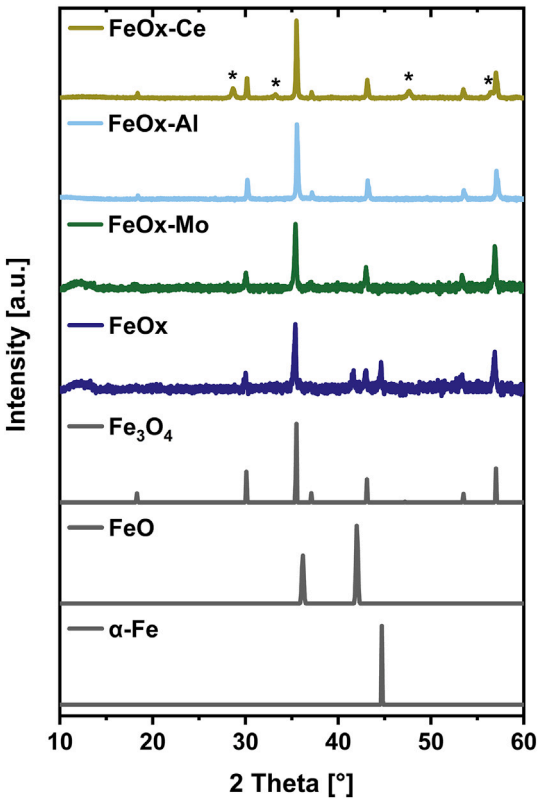

Fig. 8. XRD spectra of the samples after 5 cycles measured with Cu–K_α source with the reference spectra for Fe, FeO and Fe_3O_4. The reflexes that can be assigned to CeO_2 are marked with stars.

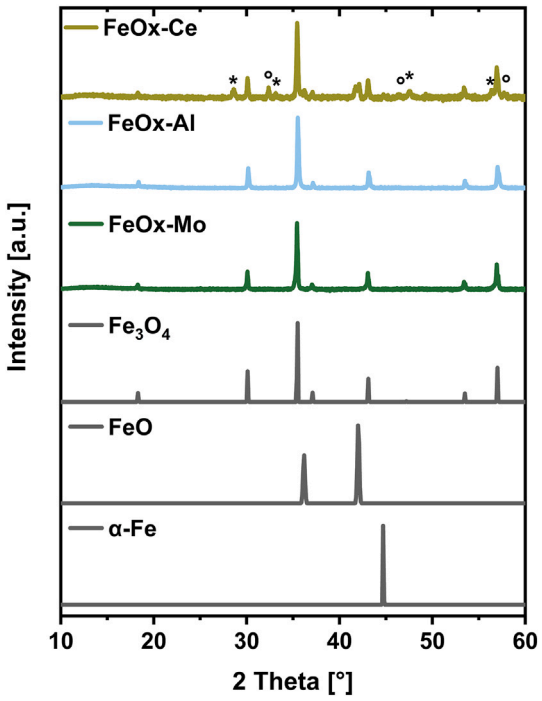

Fig. 9. XRD spectra of the samples after 16 cycles measured with Cu–K_α source with the reference spectra for Fe, FeO and Fe_3O_4. The reflexes that can be assigned to CeO_2 and $CeFeO_3$ are marked with stars or circles.

iron oxide (FeOx) exhibited incomplete oxidation after five cycles, with the presence of Fe_3O_4, FeO, and elemental iron.

In contrast, the XRD spectra of Al- and Mo-modified iron oxides showed only reflexes of Fe_3O_4, indicating complete oxidation. This conclusion is supported by the high observed hydrogen production levels, which correspond to the complete oxidation states of the modified samples. Even after 16 cycles, only Fe_3O_4 is detected in the samples modified with Mo and Al. While XRD analysis indicates complete oxidation, the observed hydrogen production is slightly below the theoretically possible amount (Fig. 7). This discrepancy may be due to several factors. One reason could be the detection limit of XRD. Small amounts of Fe or FeO might not be identifiable due to weak reflexes. Additionally, the formation of amorphous phases, which are undetectable by XRD, could contribute to the discrepancy. Another possibility is that the preceding reduction process is incomplete, resulting in less H_2 formation than expected if elemental Fe were present. The sample modified with Ce also shows traces of FeO after 16 cycles, which indicates incomplete oxidation. In addition to iron oxides, cerium species were identified. After 5 cycles, cerium is present as CeO_2, consistent with the initial synthesis. After 16 cycles, iron-cerium compounds such as $CeFeO_3$ have formed. This binding of iron to cerium reduces the hydrogen storage capacity, as the bound iron can no longer participate in the redox reaction [65]. For the samples modified with Al and Mo, the initial oxides Al_2O_3 and MoO_3 could not be identified by XRD, indicating a higher dispersivity compared to the Ce-modified sample. The formation of additive iron compounds is also likely negligible for Al and Mo under these conditions. The formation of additive iron compounds could also not be confirmed by XRD. However, missing reflexes might be influenced by fluorescence effects from the Cu X-ray source, which can increase background noise and reduce peak intensity in iron samples, potentially contributing to the absence of additive reflexes [69].

In addition to the formation of compounds that reduce the number of active iron atoms, sintering is also a crucial factor contributing to the decreased activity of the samples. To assess the extent to which the different modified oxides are affected by sintering, scanning electron microscopy (SEM) images of the fresh particles and those subjected to 16 redox cycles were taken (Fig. 10). For further quantification, the specific surface area of the initial samples and those after five and sixteen cycles was determined using the BET method (Table 3). The surface morphology of all fresh modified samples appears similar. The particles exhibit a rough and porous texture, suggesting they are composed of an agglomerate of smaller particles. Smaller particles on the surface might be the respective additive oxides. The surfaces of the samples FeOx-Al and FeOx-Mo change only slightly after 16 cycles, maintaining a porous structure comprised of numerous small particles. In contrast, the surface of FeOx-Ce shows significant sintering after 16 cycles, with the previously observed pores no longer visible.

The fact that the FeOx-Al and FeOx-Mo samples also undergo sintering is evidenced by the changes in their specific surface areas. Initially, the iron oxide modified with Al has the highest specific surface area of all the samples at 10.76 m^2g^{-1}. After five cycles, this area decreases by 82 % to 1.94 m^2g^{-1}, and after 16 cycles, it further declines to 1.67 m^2g^{-1}. The specific surface area of the iron oxide modified with Mo starts as the lowest of all samples at 2.78 m^2g^{-1}, which decreases by 71 % to 0.81 m^2g^{-1} after 16 cycles. The strongest decrease is observed with FeOx-Ce. Initially, its specific surface area is 8.02 m^2g^{-1}, which drops to 0.67 m^2g^{-1} after five cycles and further to 0.16 m^2g^{-1} after 16 cycles. This equals a 98 % decline in specific surface area. For comparison, unmodified iron oxide shows a 97 % decrease in specific surface area after only five cycles, dropping from 3.72 to 0.11 m^2g^{-1}.

However, when these results are compared with the hydrogen production of the samples (Fig. 7), it becomes clear that while specific surface area is a decisive factor for the activity of the samples, it cannot be used as the sole criterion. This conclusion is further supported by the fact that the fresh samples exhibit very different specific surface

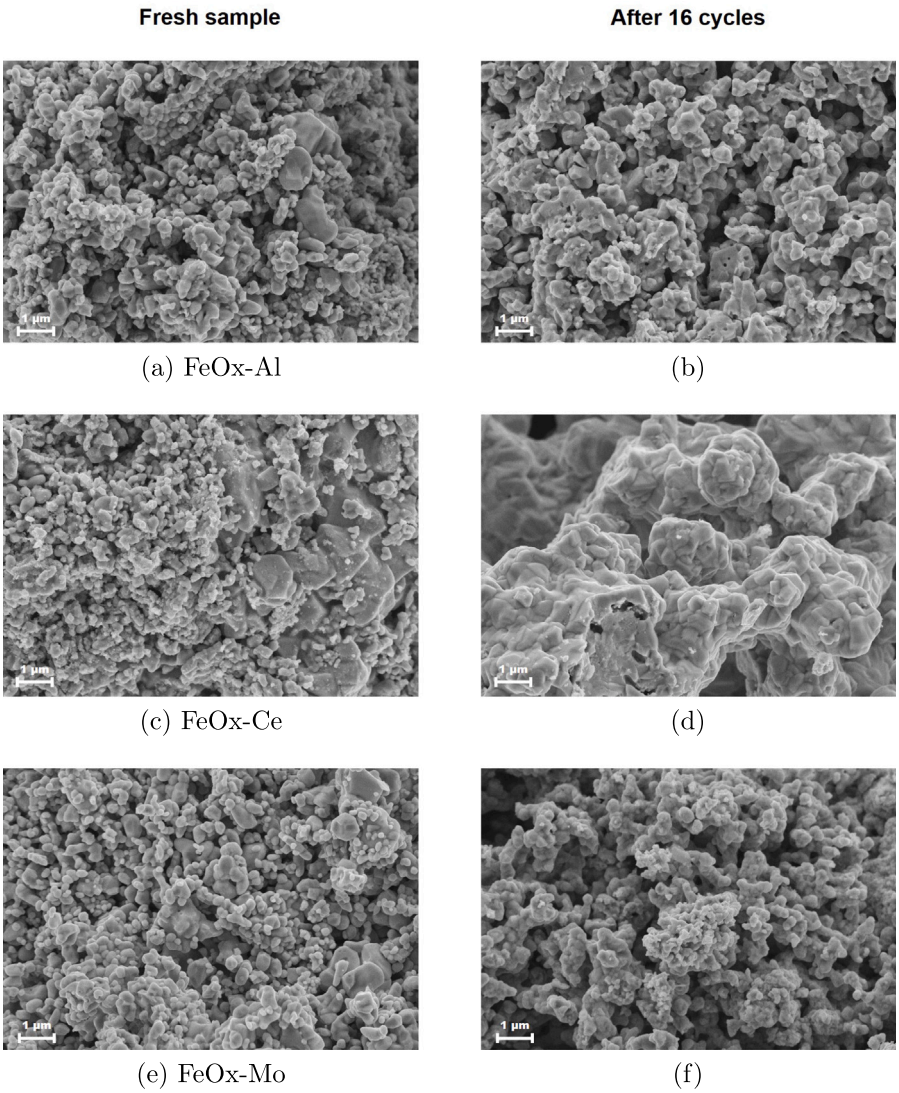

Fig. 10. SEM images of the fresh modified iron particles (left) and the respective samples after 16 redox cycles at 600 °C (right). FeOx-Ce is visibly sintered after 16 cycles (d).

Table 3
Specific surface area of the fresh unmodified iron oxide and Al-, Ce- and Mo modified iron oxides and after five and 16 cycles.

	Specific surface area [m^2g^{-1}]		
	Fresh	5 cycles	16 cycles
FeOx	3.72	0.11	–
FeOx-Al	10.76	1.94	1.67
FeOx-Ce	8.02	0.67	0.16
FeOx-Mo	2.78	–	0.81

areas, yet show comparable activity in the first cycle. Similarly, Lorente et al. [56] did not find a correlation between the specific surface area of modified iron oxide samples before cycling and their reactivity in the steam-iron process. Additionally, all samples demonstrate a significant decrease in the specific surface area up to the fifth cycle, while their activity remains approximately constant. This supports the conclusion that factors beyond specific surface area, such as the effects of additives on the reactivity, play a more critical role in maintaining redox activity over multiple cycles. Only the sample modified with Ce exhibits a drop in activity. This sample shows the most pronounced decrease in the specific surface area. However, XRD analysis of the sample after cycling has also revealed the formation of $CeFeO_3$ with further increasing cycling number, which might reduce the activity. This indicates that the decrease in activity, as well as the maintenance of activity over several cycles, is influenced by the additives, but not solely by the prevention of sintering, as described in previous literature. Instead, it can be concluded that the additives Al and Mo reduce particle sintering but cannot prevent it. Additionally, Al and Mo contribute to an increased redox activity. Otsuka et al. [42] suggest that formed compound oxides might increase the diffusion of oxide ions or activate the dissociation of H_2O or H_2.

To investigate whether this effect remains constant over a higher number of cycles, the long-term stability of the molybdenum-modified sample was studied. It is assumed that molybdenum provides enhanced stability over multiple cycles, as aluminum shows a slight decline in hydrogen production over 16 cycles. An experiment was

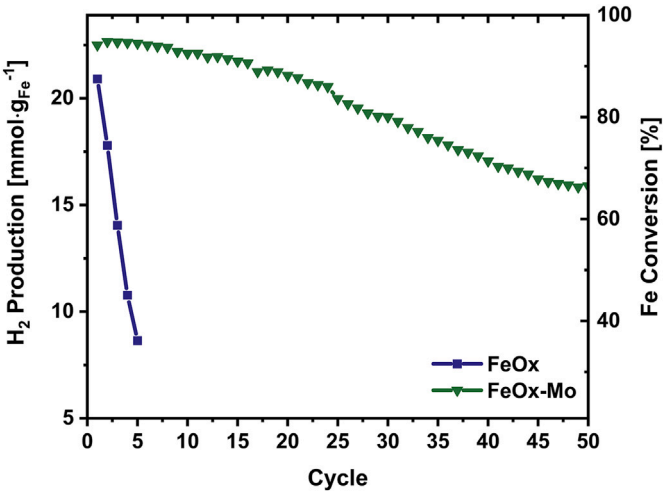

Fig. 11. Accumulated hydrogen production of iron oxide modified with Mo per cycle in the oxidation step over 50 cycles. The theoretical amount of H_2 produced by complete oxidation of Fe to Fe_3O_4 equals 23.9 mmol g_{Fe}^{-1}. Hydrogen production of FeOx-Mo declines 28 % over 50 cycles compared to a 59 % drop in five cycles without molybdenum modification.

conducted over 50 cycles at 600 °C to assess the long-term stability of FeOx-Mo. To ensure completion of the reactions, the reduction and oxidation times were extended to 180 min and 45 min, respectively.

The amount of hydrogen produced per cycle is shown in Fig. 11. In the first 10 cycles, hydrogen production remains nearly constant at approximately 22 mmol g_{Fe}^{-1}. The higher amount of hydrogen released during oxidation compared to experiments with shorter reduction times (Fig. 7) indicates, that a higher reduction degree is reached. Starting from the 10th cycle, hydrogen production decreases slightly with each subsequent cycle, reaching around 16 mmol g_{Fe}^{-1} by the 50th cycle. Over the duration of 50 redox cycles, a decline of 28 % in the amount of H_2 produced, compared to the first cycle, was observed. The change in hydrogen production per cycle indicates a gradual decline in degradation rate after the 32nd cycle, suggesting the onset of stabilization (Fig. A.19).

After 50 cycles, the fixed bed in the reactor was visibly compacted. SEM confirmed the formation of agglomerates consisting of multiple particles (Fig. 12). The pore structure of the sample subjected to cyclization is coarser compared to the fresh sample, indicating that the sample modified with Mo also undergoes visible sintering after 50 cycles (Fig. 12).

While the amount of hydrogen produced was not maintained at a constant level over 50 cycles, the introduction of molybdenum into iron oxide significantly stabilizes the hydrogen production compared to iron oxide without promoters. The impact of Mo as an additive on stabilizing the performance of the iron oxide is evident when examining the relationship between the number of cycles and the amount of hydrogen produced. Unmodified iron oxide (FeOx) experienced a 59 % decline in hydrogen production after five cycles, whereas the introduction of Mo resulted in only a 28 % decrease in hydrogen production after 50 cycles.

3.3. Redox activity of the additives

As an alternative hydrogen storage material in a metal-steam process to iron, Thaler and Hacker [6] have proposed molybdenum as a potential hydrogen storage medium. Thermodynamically, molybdenum can be oxidized to MoO_2 under the selected conditions and subsequently reduced with hydrogen. In comparison, Al_2O_3 remains thermodynamically stable under these reduction conditions. To determine whether the additives Mo and Ce not only provide stabilization, but also have an additional positive effect on the hydrogen storage performance, the reduction behavior of the modified iron oxides, FeOx-Mo and FeOx-Ce, was examined using thermogravimetric analysis (Fig. 13). However, it should be noted that, due to experimental constraints, the experimental parameters differ slightly from those of the fixed bed. The thermogravimetric analysis was not used to directly compare kinetics under identical conditions; rather, it was used to gain further insight into material behavior and additive effects. It can be observed that the mass decrease of FeOx-Ce corresponds to the reduction of Fe_2O_3 to Fe, while the Mo-modified sample exhibits a higher mass decrease, reaching up to 65 wt. – %. This mass loss corresponds to the complete reduction of both MoO_3 and Fe_2O_3 to Mo and Fe. This indicates that, in addition to the reduction of Fe_2O_3, MoO_3 is reduced, whereas CeO_2 remains in its oxide form under these reductive conditions.

To investigate the redox activity of the additives in detail, Al_2O_3, which is considered inert, was impregnated with Mo or Ce. The amount of Mo and Ce was selected to correspond to the 5 mol% additive concentration used for modifying Fe_2O_3. The samples are referred to as Al_2O_3–Mo and Al_2O_3–Ce. The tests were conducted in a fixed-bed reactor under the same conditions as those used for the investigation of the modified Fe_2O_3 samples. Fig. 14 illustrates the hydrogen production by the oxidation of Al_2O_3–Ce and Al_2O_3–Mo over five cycles. The experiments indicate that Al_2O_3–Ce undergoes minimal oxidation, whereas Al_2O_3–Mo experiences significantly more pronounced and consistent oxidation throughout the five cycles.

XRD analysis of the samples after five cycles shows that the additives are present as MoO_2 or CeO_2 (Fig. 15). Therefore, it can be assumed that

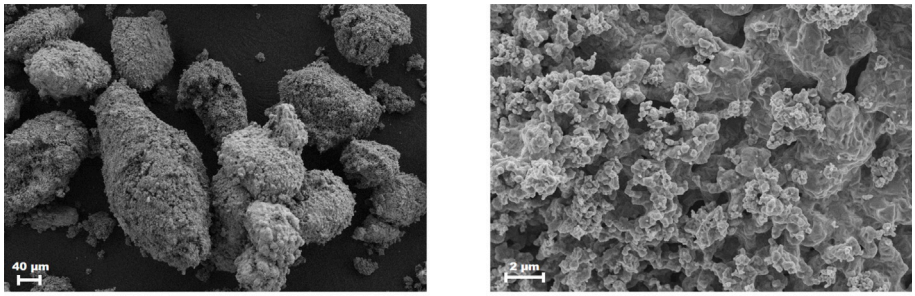

Fig. 12. SEM images of the with Mo modified iron oxide particles after 50 redox cycles at 600 °C. The formation of agglomerates consisting of multiple particles (a) and the coarsening of the pore structure (b) are shown.

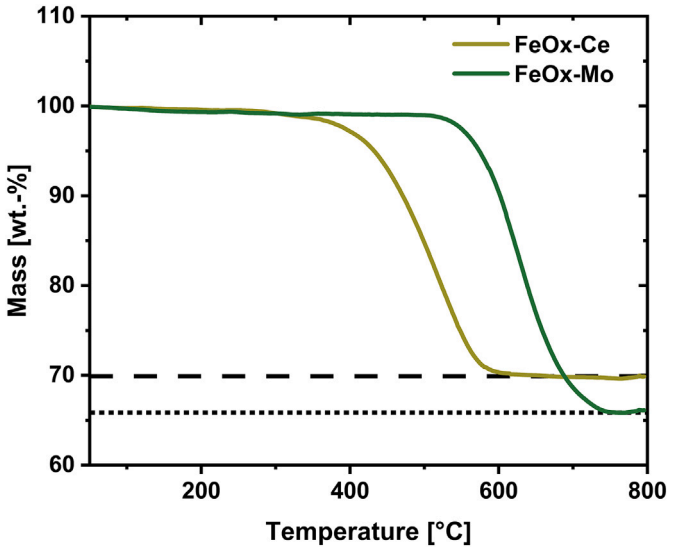

Fig. 13. TGA of the reduction of FeOx-Mo and FeOx-Ce with 10 vol. − % H_2 and a heating rate of 5 K min^{-1}. The dashed line marks the complete reduction of Fe_2O_3 to Fe and the dotted line the mass loss resulting in the additional reduction of MoO_3 to Mo.

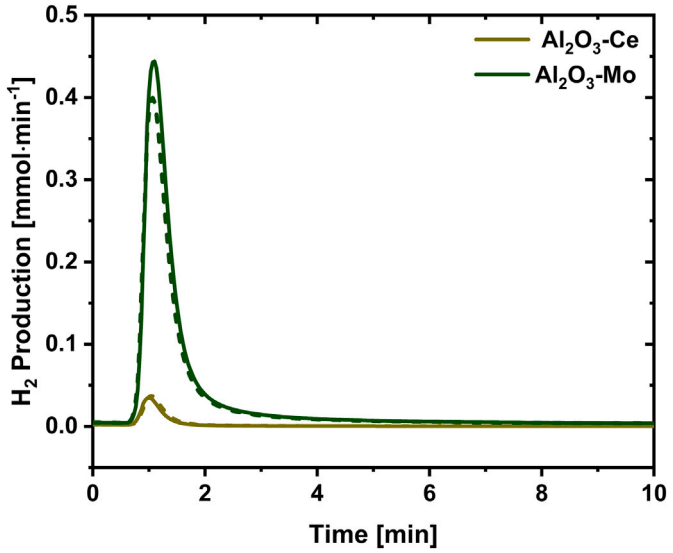

Fig. 14. Hydrogen production by the oxidation of Al_2O_3 − Ce and Al_2O_3–Mo with 20 vol. − % H_2O at 600 °C in the first (bold line) and fifth (dotted line) cycle.

the initially present MoO_3 is reduced to Mo in the first cycle and is subsequently oxidized to MoO_2 in the following cycles, as formation of MoO_3 is only reached by oxidizing with O_2. This is because the thermodynamically favoured product, MoO_2 is formed when Mo is oxidized by H_2O, whereas the formation of MoO_3 occurs only in the presence of air [6]. The fact that the amount of hydrogen produced corresponds to 60 % of the amount expected from the complete oxidation of Mo to MoO_2 indicates that a significant proportion of Mo is oxidized. The absence of elemental Mo, MoO_3, or other species in the XRD spectra could be due to their amorphous nature. Alternatively, the lack of these species could be attributed to the formation of oxygen-deficient molybdenum oxide (Mo_3O) [70].

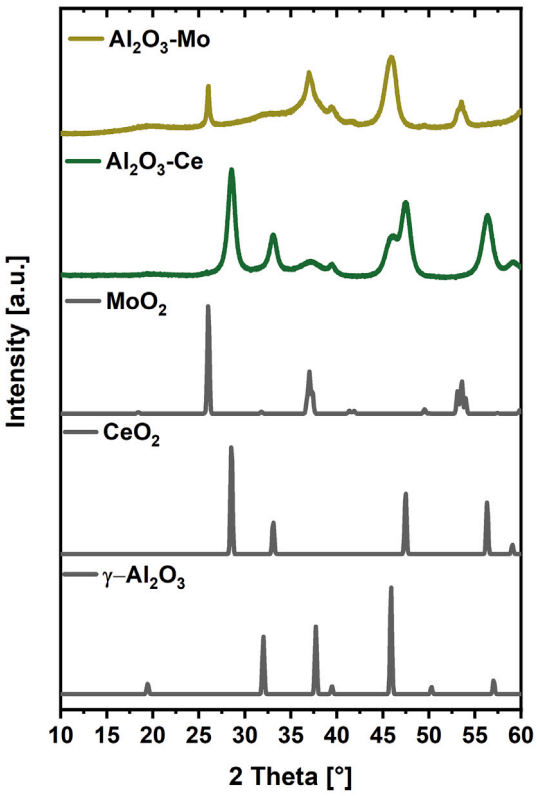

Fig. 15. XRD spectra of Al_2O_3–Ce and Al_2O_3–Mo after five cycles measured with Co-K_α source and the respective reference spectra of Al_2O_3, CeO_2 and MoO_2.

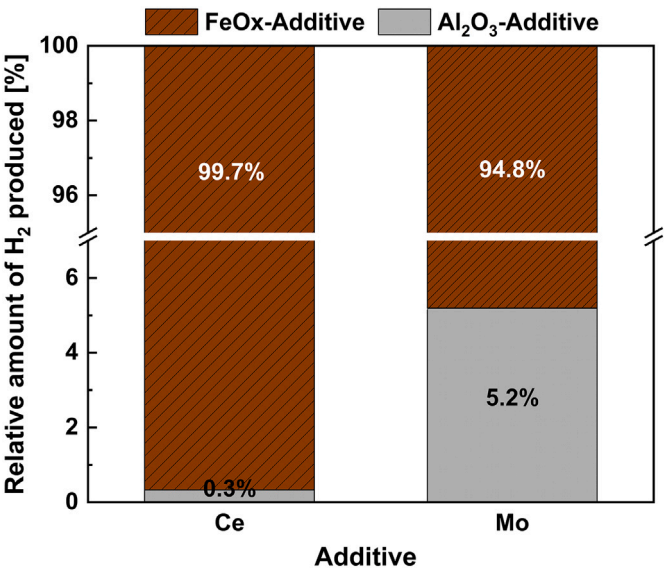

Fig. 16. Relative amount of H_2 produced by the oxidation of Al_2O_3–Mo and Al_2O_3–Ce in relation to the amount of H_2 produced by FeOx-Mo and FeOx-Ce in the first cycle.

Comparing the amount of hydrogen produced by reoxidation of Al_2O_3–Ce to that produced by the respective iron oxide sample (FeOx-Ce), it is evident that the contribution of the redox reaction of cerium oxide to the hydrogen storage capacity of FeOx-Ce is negligible, accounting for only 0.3 % of the hydrogen produced in the first cycle

(Fig. 16). In contrast, the hydrogen formed by the oxidation of Mo would correspond to 5 % of the amount of hydrogen formed by the respective iron oxide (FeOx-Mo) in the first cycle. Therefore, Mo not only stabilizes iron oxide in the steam-iron process but also enhances the hydrogen storage capacity by participating in a redox reaction. However, it should be noted that the results for Al_2O_3–Mo cannot be directly extrapolated to those for FeOx-Mo. One reason for this is the potential formation of iron molybdates, such as $FeMoO_4$, which can alter the oxidation and reduction behavior [71]. Takenaka et al. [51] confirmed the formation of ferrites ($Mo_xFe_{3-x}O_4$) by XANES for iron oxide modified with 5 % Mo after reduction and subsequent oxidation. However, no evidence of this was found in this work.

4. Conclusions

The influence of Ce, Mo and Al as additives on the stability of hydrogen production via the oxidation of iron with steam in the steam-iron process was investigated in a fixed-bed reactor. The additives contribute to an increased stability in the hydrogen production. However, the addition of Ce cannot prevent sintering as effectively as Al and Mo over several cycles. Nonetheless, it could be shown that the reduction in specific surface area is significant for all samples. Accordingly, no direct correlation can be established between activity and a high specific surface area. Both Mo and Al can stabilize hydrogen production over multiple cycles, with Mo additionally enhancing the hydrogen storage capacity due to its redox behavior. Even after 50 cycles, iron oxide modified with Mo exhibits significantly higher activity than unmodified iron oxides. The synthesis method also plays a significant role. Synthesis through impregnation increases the additive concentration on the particle surface, leading to a more effective reduction in agglomeration. The effectiveness of modifying iron oxide with a single additive makes its simultaneous modification with multiple additives an interesting approach to further improve cycle stability. Since deactivation influences both the reduction and oxidation steps, the current focus on oxidation provides a robust indicator of overall material stability. Future studies will extend this work by exploring the reduction behavior in detail, further enhancing our understanding of long-term redox performance.

CRediT authorship contribution statement

A. Knapp: Writing – original draft, Investigation, Writing – review & editing, Methodology, Conceptualization, Validation, Data curation, Visualization, Formal analysis. **C. Kuhn:** Visualization, Investigation, Writing – original draft, Methodology, Writing – review & editing, Supervision, Conceptualization, Validation, Formal analysis. **O. Deutschmann:** Project administration, Methodology, Conceptualization, Resources, Supervision, Writing – review & editing, Funding acquisition.

Declaration of generative AI and AI-assisted technologies in the writing process

During the preparation of this work the authors used ChatGPT and DeepL Write in order to improve readability. After using this tool/service, the authors reviewed and edited the content as needed and take full responsibility for the content of the publication.

Declaration of competing interest

The authors declare that they have no known competing financial interests or personal relationships that could have appeared to influence the work reported in this paper.

Acknowledgements

This work was performed within the cluster project Clean Circles. Financial support by the Strategy Fund of the KIT Presidium is gratefully acknowledged. We thank the NFDI4Cat consortium, funded by Deutsche Forschungsgemeinschaft (DFG, German Research Foundation) through project 441926934, for cost-free use of the research data management software Adacta, and the omegadot software & consulting GmbH for support in installation and application of Adacta. The authors thank Dr. Thomas Bergfeldt (IAM, KIT) for the ICP-OES analysis and Lukas Braun (ITCP, KIT), Petra Schlager (IMB, KIT) and Özge Selcuk (TU Bergakademie Freiberg) for XRD analysis.

Appendix A. Appendix section

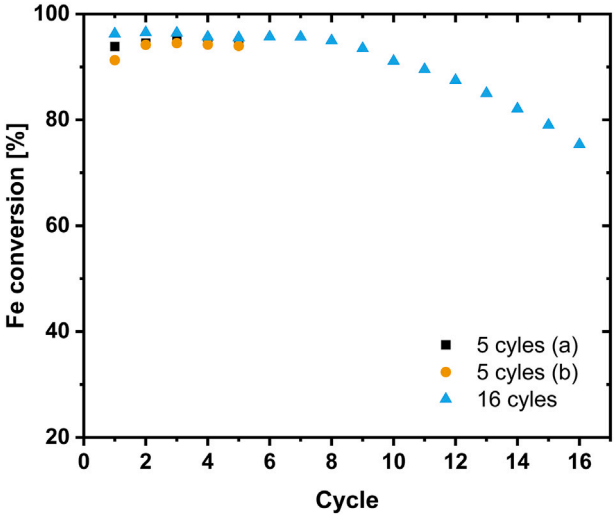

Fig. A.17. Accumulated hydrogen production per cycle during the oxidation step for Ce-modified iron oxide (FeOx-Ce). The five-cycle tests were repeated twice, showing good reproducibility, while the 16-cycle experiment was conducted once. The hydrogen yields observed in the 16-cycle test align well with those of the repeated five-cycle experiments, further supporting the consistency of the results.

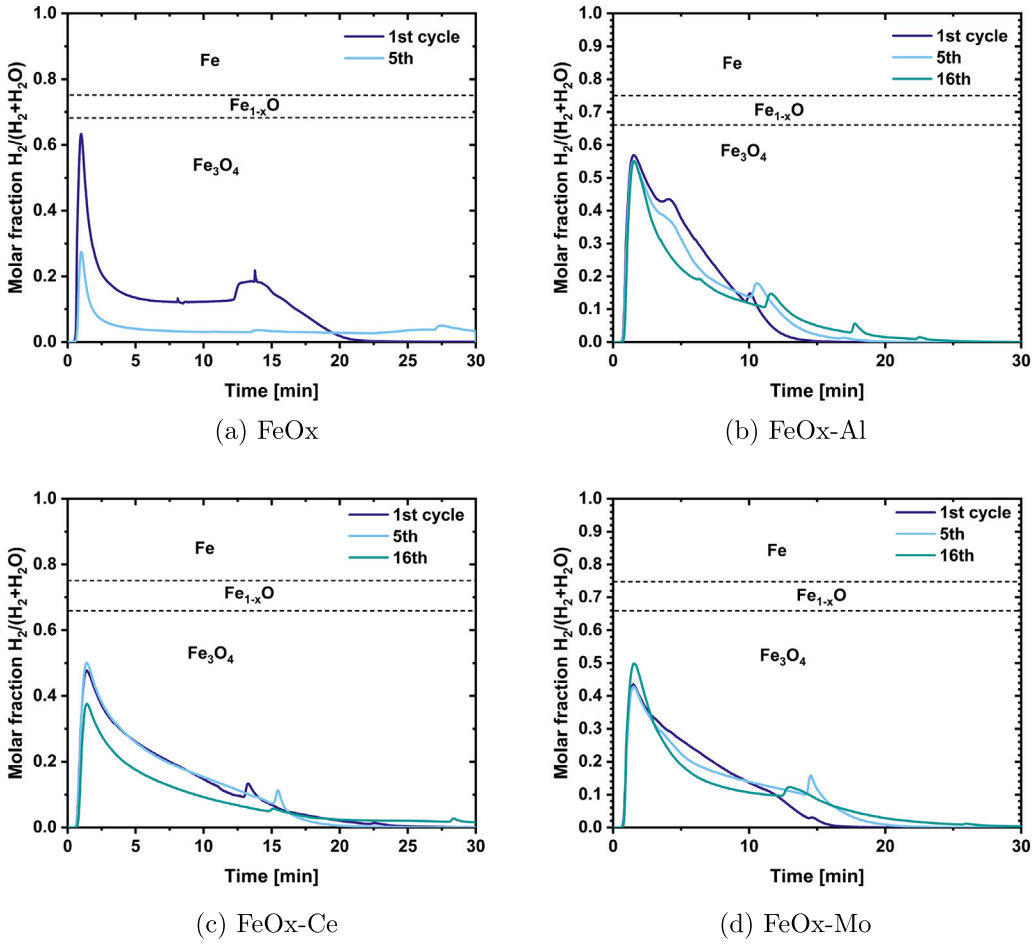

Fig. A.18. $H_2 \setminus (H_2 + H_2O)$ ratio during oxidation with 20 vol.−% H_2O at 600 °C of the none-modified iron oxide and the modified iron oxides over time. The dashed lines mark the solid-phase equilibrium between iron and its oxides in the Fe–H–O system at 600 °C. This representation allows direct comparison with the Bauer-Glaessner diagram (Fig. 3) and confirms that the oxidation conditions consistently remain within the Fe_3O_4 stability regime. The low $H_2 \setminus (H_2 + H_2O)$ ratios throughout the oxidation steps indicate that the reaction was not limited by thermodynamic equilibrium under the applied conditions.

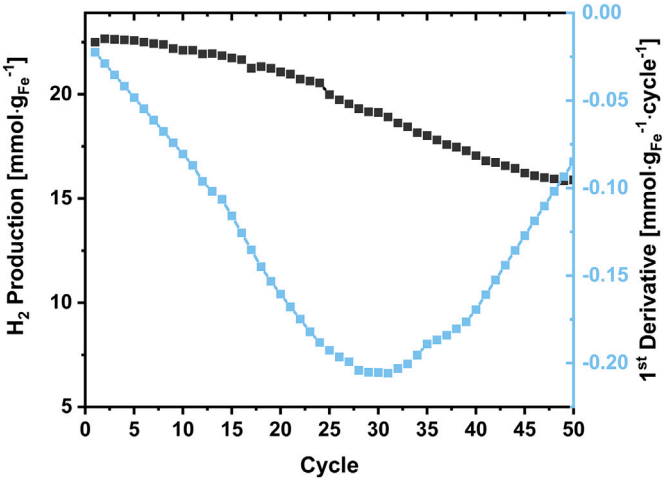

Fig. A.19. Accumulated hydrogen production per cycle and its first derivative during the oxidation step for Mo-modified iron oxide over 50 redox cycles. The theoretical amount of H_2 produced by complete oxidation of Fe to Fe_3O_4 equals 23.9 mmol $g_{Fe}{}^{-1}$. The derivative illustrates a decreasing rate of degradation, with the decline in hydrogen production per cycle gradually diminishing after approximately 32 cycles.

Data availability

Data will be made available upon request.

References

[1] Li Y, Chen H, Zhang X, Tan C, Ding Y. Renewable energy carriers: hydrogen or liquid air/nitrogen? Appl Therm Eng 2010;30:1985–90. https://doi.org/10.1016/j.applthermaleng.2010.04.033.

[2] Møller KT, Jensen TR, Akiba E, Li H-W. Hydrogen - a sustainable energy carrier. Prog Nat Sci Mater Int 2017;27:34–40. https://doi.org/10.1016/j.pnsc.2016.12.014.

[3] Andersson J, Grönkvist S. Large-scale storage of hydrogen. Int J Hydrog Energy 2019;44:11901–19. https://doi.org/10.1016/j.ijhydene.2019.03.063.

[4] Mazloomi K, Gomes C. Hydrogen as an energy carrier: prospects and challenges. Renew Sustain Energy Rev 2012;16:3024–33. https://doi.org/10.1016/j.rser.2012.02.028.

[5] Orimo S-I, Nakamori Y, Eliseo JR, Züttel A, Jensen CM. Complex hydrides for hydrogen storage. Chem Rev 2007;107:4111–32. https://doi.org/10.1021/cr0501846.

[6] Thaler M, Hacker V. Storage and separation of hydrogen with the metal steam process. Int J Hydrog Energy 2012;37:2800–06. https://doi.org/10.1016/j.ijhydene.2011.06.119.

[7] Moradi R, Groth KM. Hydrogen storage and delivery: review of the state of the art technologies and risk and reliability analysis. Int J Hydrog Energy 2019;44:12254–69. https://doi.org/10.1016/j.ijhydene.2019.03.041.

[8] Davari S, Cárdenas C, Hettel M, Lott P, Tischer S, Angeli S, et al. Spatially resolved measurements in a stagnation-flow reactor: kinetics of catalytic NH_3 decomposition. Chem Ing Tech 2024;96:1735–50. https://doi.org/10.1002/cite.202400100.

[9] Lamb KE, Dolan MD, Kennedy DF. Ammonia for hydrogen storage; a review of catalytic ammonia decomposition and hydrogen separation and purification. Int J Hydrogen Energy 2019;44:3580–93. https://doi.org/10.1016/j.ijhydene.2018.12.024

[10] Preuster P, Papp C, Wasserscheid P. Liquid organic hydrogen carriers (LOHCs): toward a hydrogen-free hydrogen economy. Acc Chem Res 2017;50:74–85. https://doi.org/10.1021/acs.accounts.6b00474.

[11] Markiewicz M, Zhang YQ, Bösmann A, Brückner N, Thöming J, Wasserscheid P, et al. Environmental and health impact assessment of liquid organic hydrogen carrier (LOHC) systems – challenges and preliminary results. Energy Environ Sci 2015;8:1035–45. https://doi.org/10.1039/C4EE03528C.

[12] Markiewicz M, Zhang Y-Q, Empl MT, Lykaki M, Thöming J, Steinberg P, et al. Hazard assessment of quinaldine-, alkylcarbazole-, benzene- and toluene-based liquid organic hydrogen carrier (LOHCs) systems. Energy Environ Sci 2019;12:366–83. https://doi.org/10.1039/C8EE01696H.

[13] Düll A, Rohlfs P, Deutschmann O, Börnhorst M. Performance evaluation of KBH_4 as Energy carrier for shipping applications. Chem Ing Tech 2022;94:747–59. https://doi.org/10.1002/cite.202100193.

[14] Jain I, Lal C, Jain A. Hydrogen storage in Mg: a most promising material. Int J Hydrog Energy 2010;35:5133–44. https://doi.org/10.1016/j.ijhydene.2009.08.088.

[15] Usman MR. Hydrogen storage methods: review and current status. Renew Sustain Energy Rev 2022;167:112743. https://doi.org/10.1016/j.rser.2022.112743.

[16] Klopčič N, Grimmer I, Winkler F, Sartory M, Trattner A. A review on metal hydride materials for hydrogen storage. J Energy Storage 2023;72:108456. https://doi.org/10.1016/j.est.2023.108456.

[17] Brinkman L, Bulfin B, Steinfeld A. Thermochemical hydrogen storage via the reversible reduction and oxidation of metal oxides. Energy Fuels 2021;35:18756–67. https://doi.org/10.1021/acs.energyfuels.1c02615.

[18] Bergthorson J, Goroshin S, Soo M, Julien P, Palecka J, Frost D, et al. Direct combustion of recyclable metal fuels for zero-carbon heat and power. Appl Energy 2015;160:368–82. https://doi.org/10.1016/j.apenergy.2015.09.037.

[19] Bergthorson JM. Recyclable metal fuels for clean and compact zero-carbon power. Prog Energy Combust Sci 2018;68:169–96. https://doi.org/10.1016/j.pecs.2018.05.001.

[20] Mi X, Fujinawa A, Bergthorson JM. A quantitative analysis of the ignition characteristics of fine iron particles. Combust Flame 2022;240:112011. https://doi.org/10.1016/j.combustflame.2022.112011.

[21] Ning D, Hazenberg T, Shoshin Y, Van Oijen J, Finotello G, De Goey L. Experimental and theoretical study of single iron particle combustion under low-oxygen dilution conditions. Fuel 2024;357:129718. https://doi.org/10.1016/j.fuel.2023.129718.

[22] Debiagi P, Rocha R, Scholtissek A, Janicka J, Hasse C. Iron as a sustainable chemical carrier of renewable energy: analysis of opportunities and challenges for retrofitting coal-fired power plants. Renew Sustain Energy Rev 2022;165:112579. https://doi.org/10.1016/j.rser.2022.112579.

[23] Neumann J, Fradet Q, Scholtissek A, Dammel F, Riedel U, Dreizler A, et al. Thermodynamic assessment of an iron-based circular energy economy for carbon-free power supply. Appl Energy 2024;368:123476. https://doi.org/10.1016/j.apenergy.2024.123476.

[24] Auner N, Holl S. Silicon as energy carrier—facts and perspectives. Energy 2006;31:1395–402. https://doi.org/10.1016/j.energy.2005.12.001.

[25] Kuhn C, Düll A, Rohlfs P, Tischer S, Börnhorst M, Deutschmann O. Iron as recyclable energy carrier: feasibility study and kinetic analysis of iron oxide reduction. Appl Energy Combust Sci 2022;12:100096. https://doi.org/10.1016/j.jaecs.2022.100096.

[26] Kuhn C, Kirn M, Tischer S, Deutschmann O. Micron-sized iron particles as energy carrier: cycling experiments in a fixed-bed reactor. Proc Combust Inst 2024;40:105207. https://doi.org/10.1016/j.proci.2024.105207.

[27] Trowell K, Goroshin S, Frost D, Bergthorson J. Aluminum and its role as a recyclable, sustainable carrier of renewable energy. Appl Energy 2020;275:115112. https://doi.org/10.1016/j.apenergy.2020.115112.

[28] Teichert M, Haller MY, Sick F. Aluminium redox cycle in comparison to pressurized hydrogen for the energy supply of multi-family houses. Appl Energy Combust Sci 2023;13:100098. https://doi.org/10.1016/j.jaecs.2022.100098.

[29] Barelli L, Baumann M, Bidini G, Ottaviano PA, Schneider RV, Passerini S, et al. Reactive metals as energy storage and carrier media: use of aluminum for power generation in fuel cell-based power plants. Energy Technol 2020;8:2000233. https://doi.org/10.1002/ente.202000233.

[30] Shkolnikov E, Zhuk A, Vlaskin M. Aluminum as energy carrier: feasibility analysis and current technologies overview. Renew Sustain Energy Rev 2011;15:4611–23. https://doi.org/10.1016/j.rser.2011.07.091

[31] Baumann M, Barelli L, Passerini S. The potential role of reactive metals for a clean energy transition. Adv Energy Mater 2020;10:2001002. https://doi.org/10.1002/aenm.202001002.

[32] Kuhn C, Knapp A, Deutschmann MP, Spielmann J, Tischer S, Kramm UI, et al. Iron as recyclable metal fuel: unraveling oxidation behavior and cyclization effects through Thermogravimetric analysis, wide-angle X-ray scattering and Mössbauer spectroscopy. ChemSuschem 2024;17:e202400351. https://doi.org/10.1002/cssc.202400351.

[33] Messerschmitt A. Process of producing hydrogen. 1910; US Pat., US971206A.

[34] Hurst S. Production of hydrogen by the steam-iron method. Oil Soap 1939;16:29–35. https://doi.org/10.1007/BF02543209.

[35] Block F, Speicher R, Kollers G. Der Eisen-Dampf-Prozeß zur Wasserstofferzeugung. Arch für das Eisenhüttenwesen 1983;54:129–32. https://doi.org/10.1002/srin.198305212.

[36] Hacker V. A novel process for stationary hydrogen production: the reformer sponge iron cycle (RESC). J Power Sour 2003;118:311–14. https://doi.org/10.1016/S0378-7753(03)00076-4.

[37] Lorente E, Cai Q, Peña J, Herguido J, Brandon N. Conceptual design and modelling of the steam-iron process and fuel cell integrated system. Int J Hydrog Energy 2009;34:5554–62. https://doi.org/10.1016/j.ijhydene.2009.04.062.

[38] Mignard D, Pritchard C. A review of the sponge iron process for the storage and transmission of remotely generated marine energy. Int J Hydrog Energy 2007;32:5039–49. https://doi.org/10.1016/j.ijhydene.2007.06.032.

[39] Pineau A, Kanari N, Gaballah I. Kinetics of reduction of iron oxides by H2. Thermochim Acta 2006;447:89–100. https://doi.org/10.1016/j.tca.2005.10.004.

[40] Neumann J, Da Rocha RC, Debiagi P, Scholtissek A, Dammel F, Stephan P, et al. Techno-economic assessment of long-distance supply chains of energy carriers: comparing hydrogen and iron for carbon-free electricity generation. Appl Energy Combust Sci 2023;14:100128. https://doi.org/10.1016/j.jaecs.2023.100128.

[41] Galvita V, Sundmacher K. Hydrogen production from methane by steam reforming in a periodically operated two-layer catalytic reactor. Appl Catal A Gener 2005;289:121–27. https://doi.org/10.1016/j.apcata.2005.04.053.

[42] Otsuka K, Yamada C, Kaburagi T, Takenaka S. Hydrogen storage and production by redox of iron oxide for polymer electrolyte fuel cell vehicles. Int J Hydrogen Energy 2003;28:335–42. https://doi.org/10.1016/S0360-3199(02)00070-8.

[43] Heiniger SP, Fan Z, Lustenberger UB, Stark WJ. Safe seasonal energy and hydrogen storage in a 1:10 single-household-sized pilot reactor based on the steam-iron process. Sustain Energy Fuels 2024;8:125–32. https://doi.org/10.1039/D3SE01228J.

[44] Lorente E, Pena JA, Herguido J. Kinetic study of the redox process for separating and storing hydrogen: oxidation stage and ageing of solid. Int J Hydrog Energy 2008;33:615–26. https://doi.org/10.1016/j.ijhydene.2007.09.026.

[45] Bleeker M, Veringa H, Kersten S. Deactivation of iron oxide used in the steam-iron process to produce hydrogen. Appl Catal A Gener 2009;357:5–17. https://doi.org/10.1016/j.apcata.2008.12.032.

[46] Stehle R, Bobek M, Hooper R, Hahn D. Oxidation reaction kinetics for the steam-iron process in support of hydrogen production. Int J HydrogEnergy 2011;36:15125–35. https://doi.org/10.1016/j.ijhydene.2011.08.074.

[47] Otsuka K, Kaburagi T, Yamada C, Takenaka S. Chemical storage of hydrogen by modified iron oxides. J Power Sour 2003;122:111–21. https://doi.org/10.1016/S0378-7753(03)00398-7.

[48] Ryu J-C, Lee D-H, Kang K-S, Park C-S, Kim J-W, Kim Y-H. Effect of additives on redox behavior of iron oxide for chemical hydrogen storage. J Ind Eng Chem 2008;14:252–60. https://doi.org/10.1016/j.jiec.2007.10.003.

[49] De Filippis P, D'Alvia L, Damizia M, Caprariis B, Del Prete Z. Pure hydrogen production by steam-iron process: the synergic effect of MnO_2 and Fe_2O_3. Int J Energy Res 2021;45:4479–94. https://doi.org/10.1002/er.6117.

[50] Wang H, Wang G, Wang X, Bai J. Hydrogen production by redox of cation-modified iron oxide. J Phys Chem C 2008;112:5679–88. https://doi.org/10.1021/jp711587m.

[51] Takenaka S, Kaburagi T, Yamada C, Nomura K, Otsuka K. Storage and supply of hydrogen by means of the redox of the iron oxides modified with Mo and Rh species. J Catal 2004;228:66–74. https://doi.org/10.1016/j.jcat.2004.08.027.

[52] Bohn CD, Cleeton JP, Müller CR, Chuang SY, Scott SA, Dennis JS. Stabilizing iron oxide used in cycles of reduction and oxidation for hydrogen production. Energy Fuels 2010;24:4025–33. https://doi.org/10.1021/ef100199f.

[53] Nestl S, Voitic G, Lammer M, Marius B, Wagner J, Hacker V. The production of pure pressurised hydrogen by the reformer-steam iron process in a fixed bed reactor system. J Power Sour 2015;280:57–65. https://doi.org/10.1016/j.jpowsour.2015.01.052.

[54] Kidambi PR, Cleeton JPE, Scott SA, Dennis JS, Bohn CD. Interaction of iron oxide with alumina in a composite oxygen carrier during the production of hydrogen by chemical looping. Energy Fuels 2012;26:603–17. https://doi.org/10.1021/ef200859d.

[55] Bohn CD, Müller CR, Cleeton JP, Hayhurst AN, Davidson JF, Scott SA, et al. Production of very pure hydrogen with simultaneous capture of carbon dioxide using the redox reactions of iron oxides in packed beds. Ind Eng Chem Res 2008;47:7623–30. https://doi.org/10.1021/ie800335j.
[56] Lorente E, Peña J, Herguido J. Separation and storage of hydrogen by steam-iron process: effect of added metals upon hydrogen release and solid stability. J Power Sour 2009;192:224–29. https://doi.org/10.1016/j.jpowsour.2008.12.116.
[57] Gossler H, Riedel J, Daymo E, Chacko R, Angeli S, Deutschmann O. A New approach to Research data management with a focus on traceability: Adacta. Chem Ing Tech 2022;94:1798–807. https://doi.org/10.1002/cite.202200064.
[58] Spreitzer D, Schenk J. Reduction of iron oxides with hydrogen—A review. Steel Res Int 2019;90:1900108. https://doi.org/10.1002/srin.201900108.
[59] Fradet Q, Kurnatowska M, Riedel U. Thermochemical reduction of iron oxide powders with hydrogen: review of selected thermal analysis studies. Thermochim Acta 2023;726:179552. https://doi.org/10.1016/j.tca.2023.179552.
[60] Choisez L, Hemke K, Özgün Ö, Pistidda C, Jeppesen H, Raabe D, et al. Hydrogen-based direct reduction of combusted iron powder: deep pre-oxidation, reduction kinetics and microstructural analysis. Acta Mater 2024;268:119752. https://doi.org/10.1016/j.actamat.2024.119752.
[61] Cavaliere P, Dijon L, Laska A, Koszelow D. Hydrogen direct reduction and reoxidation behaviour of high-grade pellets. Int J Hydrog Energy 2024;49:1235–54. https://doi.org/10.1016/j.ijhydene.2023.08.254.
[62] Kourkoumelis N. PowDLL, a reusable.NET component for interconverting powder diffraction data: recent developments. In: Powder diffraction, vol. 28; 2013. p. 137–48. https://doi.org/10.1017/S0885715613000390.
[63] Zagorac D, Müller H, Ruehl S, Zagorac J, Rehme S. Recent developments in the inorganic crystal structure database: theoretical crystal structure data and related features. J Appl Crystallogr 2019;52:918–25. https://doi.org/10.1107/S160057671900997X.
[64] Le Page JF, Cosyns J, Courty P. Applied heterogeneous catalysis. Design-manufacture use of solid catalysts. Paris: Institut Français du Pétrole publications, Éditions Technip; 1987.
[65] Galvita V, Hempel T, Lorenz H, Rihko-Struckmann LK, Sundmacher K. Deactivation of modified iron oxide materials in the cyclic water gas shift process for CO-free hydrogen production. Ind Eng Chem Res 2008;47:303–10. https://doi.org/10.1021/ie0708879.
[66] Lok M. Coprecipitation. In: Synthesis of solid catalysts. John Wiley & Sons, Ltd; 2009. p. 135–51. https://doi.org/10.1002/9783527626854.ch7, section: 7.
[67] Marceau E, Carrier X, Che M. Impregnation and drying. In: Synthesis of solid catalysts. John Wiley & Sons, Ltd; 2009. p. 59–82. https://doi.org/10.1002/9783527626854.ch4, section: 4.
[68] Yao D, Yang H, Chen H, Williams PT. Co-precipitation, impregnation and so-gel preparation of Ni catalysts for pyrolysis-catalytic steam reforming of waste plastics. Appl Catal B Environ 2018;239:565–77. https://doi.org/10.1016/j.apcatb.2018.07.075.
[69] Mos YM, Vermeulen AC, Buisman CJN, Weijma J. X-Ray diffraction of iron containing samples: the importance of a suitable configuration. Geomicrobiol J 2018;35:511–7. https://doi.org/10.1080/01490451.2017.1401183.
[70] Schönberg N. On the existence of a metallic molybnemum oxide. Acta Chem Scand 1954;8:617–9.
[71] Trifiro F. Nature of the active component in a Fe_2O_3 MoO_3 catalyst: study on the catalyst reduction and oxidation. J Catal 1969;15:8–16. https://doi.org/10.1016/0021-9517(69)90003-7.